Journal of Alloys and Compounds 502 (2010) 107–111

Contents lists available at ScienceDirect

Journal of Alloys and Compounds

journal homepage: www.elsevier.com/locate/jallcom

Core and shell structure of ytterbium sesquioxide nanoparticles

Milica Vucinic-Vasic[a], Aleksandar Kremenovic[b], Aleksandar S. Nikolic[c], Philippe Colomban[d], Leo Mazzerolles[e], Volker Kahlenberg[f], Bratislav Antic[b,*]

[a] Faculty of Technical Sciences, University of Novi Sad, Trg D. Obradovica 6, 21000 Novi Sad, Serbia
[b] Institute of Nuclear Sciences "Vinca", Solid State Physics Laboratory, POB 522, 11001 Belgrade, Serbia
[c] Faculty of Chemistry, Department of Inorganic Chemistry, University of Belgrade, POB158, 11001 Belgrade, Serbia
[d] LADIR, UMR 7075 CNRS, and Université Pierre and Marie Curie, 94230 Thiais, France
[e] ICMPE, UMR 7182-CNRS, and Paris 12, 2-8 rue H. Dunant, 94230 Thiais, France
[f] Institute of Mineralogy and Petrography, University of Innsbruck, Innrain 52, A-6020 Innsbruck, Austria

ARTICLE INFO

Article history:
Received 15 September 2009
Received in revised form 16 March 2010
Accepted 18 March 2010
Available online 25 March 2010

Keywords:
Nanostructured materials
Chemical synthesis
Microstructure
Crystal structure
X-ray diffraction

ABSTRACT

This paper reports results concerning the crystal structure of core and shell as well as microstructure of 25 nm-ytterbium sesquioxide (Yb_2O_3) nanoparticles synthesized using a unique method based on thermal decomposition of a 2,4 pentadione complex. Used Raman spectroscopy measurements indicate core/shell structure, with monoclinic or a mixture of monoclinic and cubic symmetry of the particle shell. In addition, XRPD and SAED confirmed bixbyite structure type for the core (space group $Ia\bar{3}$). Broadening of the observed Raman bands indicates structural distortions in the nanocrystalline sample. The size/strain analysis was done on XRPD data using Fullprof/MarqX approach. Anisotropy of X-ray line broadening is caused by size effects only. The resulting mean microstrain (6×10^{-4}) points to a low concentration of defects within the crystallites.

1. Introduction

Nanocrystalline rare-earth oxides (RE_2O_3) have physical and chemical properties suitable for various applications such as phosphors, catalysts or catalyst supports, fuel cells, solid electrolytes and sintering additives in the steel industry [1]. It is known that their properties strongly depend on numerous factors such as structure, microstructure (particle shape and size, particle morphology, anisotropy), inter-particle interactions, etc. On the other hand, microstructure and structure parameters strongly depend on the preparation method used. To date, much effort has been expended in controlling the size, shape and crystal structure of rare-earth oxides to improve their properties.

Recently, a new synthesis method based on acetil-acetonato (2,4 pentadione) complexes for preparation of pure and mixed sesquioxides of the rare-earth elements crystallizing in the so-called bixbyite structure type is developed [2]. Due to the extreme importance of controlled synthesis in technology, the method was further developed and applied for preparation of ytterbium sesquioxide, which is an important material in optoelectronic devices [3].

Nanoparticles have unique physical properties as a consequence of dimensional reduction. Their properties are either significantly modified or completely new and not even present in the bulk counterpart. Nanoparticles may be core and shell structured, with amorphous or crystalline (different in size) shell. Experimental data (e.g. photoluminescence in rare-earth oxides nanophosphors, reduction or enhancement saturation magnetization and coercivity in magnetic nanoparticles) are often explained by existence of particle core and shell, but there are no systematic studies on structure of nanoparticle shell. One of the aims of the present work is a study of structure of particles shell.

This paper reports: (a) core/shell structure of nanoparticles studied by combining XRPD and Raman spectroscopy techniques, (b) microstructure of the obtained nanostructured material by suitable choice of experimental techniques (X-ray powder diffraction data – XRPD, High Resolution Transmission Electron microscopy – HRTEM and Raman spectroscopy), along with computer programs using various theoretical models for size/strain analysis from XRPD data and (c) the synthesis procedure for ytterbium sesquioxide by using a unique method.

2. Material and methods

The synthesis of Yb_2O_3 nanopowder was based on the thermal decomposition of an appropriate complex compound with acetylacetone (acac)–(2,4 pentadione) ligands ($Yb(AA)_3$). A 0.01 mol of $YbCl_3 \times 6H_2O$ was dissolved in minimum amount

* Corresponding author. Fax: +381 118065829.
E-mail address: bantic@vinca.rs (B. Antic).

0925-8388/$ – see front matter © 2010 Elsevier B.V. All rights reserved.
doi:10.1016/j.jallcom.2010.03.158

of water. A 0.03 moles of freshly prepared solution of ammonium–acetylacetonate (made by adding concentrate ammonia to acetylacetonate) was added slowly under permanent stirring. The pH was adjusted close to 6 using either diluted ammonia or diluted hydrochloric acid. After the reaction has finished, the crystalline precipitate was allowed to cool in a refrigerator at +4° C for 24 h, subsequently filtered using a Buchner's funnel and finally washed with cold water. The obtained complex $Yb(AA)_3$ was re-crystallized and dried in a vacuum dessicator. The $Yb(AA)_3$ powder was milled and then heated in a furnace in air with a heating rate of 10 °C/min up to 550 °C. The resulting material was kept at the final temperature for 1 min, and then cooled with 20 °C/min rate down to the room temperature.

To check for possible hydration of Yb_2O_3, an IR spectrum was recorded. Absence of 1640 cm^{-1} mode clearly indicates that hydration process could be excluded.

X-ray powder diffraction data (XRPD) were collected on a Stoe STADI MP diffractometer. The diffractometer is equipped with an asymmetric primary beam Ge(1 1 1) monochromator (yielding a strictly monochromatic CuKα1-radiation) and a linear PSD with 5° detector range. The samples were measured in symmetric flat-plate transmission geometry using a round sample of 2 mm diameter. The data were collected in the angular range 5–130° (2θ) with a step size of 0.01° and a counting time of 40 s per step.

A high sensitivity multichannel notch-filtered INFINITY and edge-filtered HR800 spectrograph (Jobin-Yvon–Horiba SAS, Longjumeau, France) equipped with a Peltier cooled CCD matrix detector was employed to record Raman spectra between ~150 and 2000 cm^{-1}, using 488, 514 and 632 nm excitation lines (Ar+ air cooled, Nd:YAG and He–Ne lasers).

Microstructure was investigated by HRTEM on a TOPCON 002B electron microscope operated at 200 kV.

3. Results and discussion

3.1. Crystal structure/microstructure of Yb_2O_3 nanoparticles

Synthesized sample was checked by XRPD. All reflections in the diffraction pattern were indexed in the cubic unit cell, space group $Ia\bar{3}$. The obtained results of the Rietveld refinement of the structure model described in space group $Ia\bar{3}$ [4] are in accordance with the literature data contained in the ICSD database [5] (see Fig. 1). Attempts to refine other low-symmetry structure models obtained from group-subgroup relations (including monoclinic symmetry, see also Raman part) were unsuccessful. Low background intensity values point to absence of amorphous phase. The refined value of lattice parameter is $a = 10.43970\,(6)$Å.

The morphology and particle size of Yb_2O_3 were determined by HRTEM, Fig. 2. Analysis of HRTEM picture reveals that the particles are nearly spherical in shape, with a relatively narrow size distribution and mean particle size of ~25 nm. Morphologically, no amount of amorphous phase was detected in the sample. Indexing of the selected area of the electron diffraction pattern is in accord with the XRPD results.

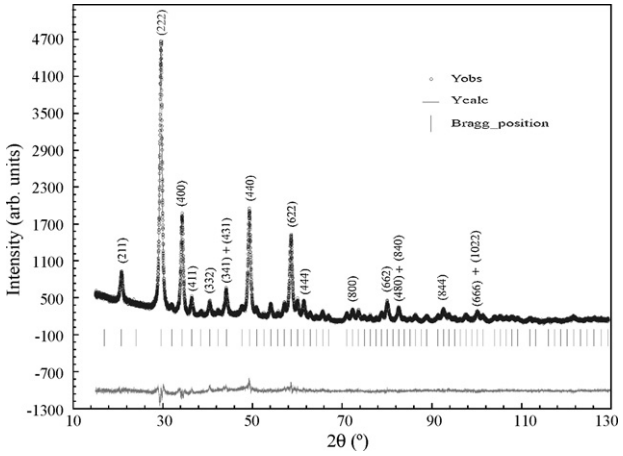

Fig. 1. Result of the Rietveld refinement for nanosized Yb_2O_3 ($R_p = 15\%$, $R_{wp} = 15.2\%$, $R_B = 8\%$, $\chi^2 = 1.54$). Dots denote observed step intensities; the line represents the corresponding calculated values. The difference curve between observed and calculated values is given at the bottom.

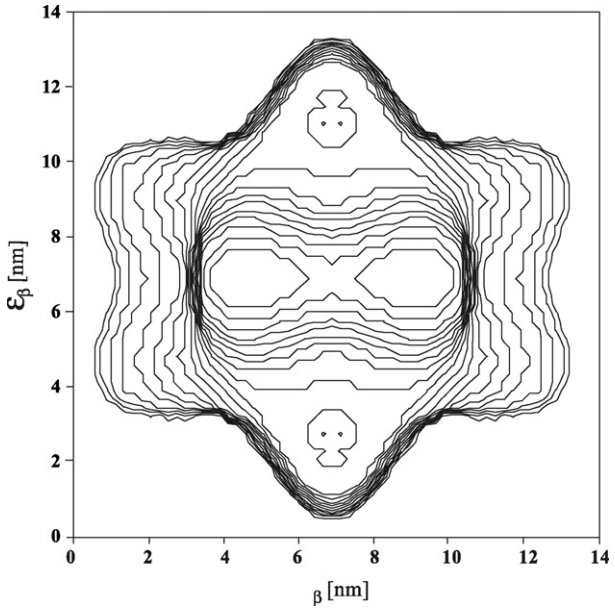

Fig. 2. Projections of the apparent crystallite size on the (0 0 1) plane for nanosized Yb_2O_3.

3.2. Crystallite size and strain in Yb_2O_3 nanoparticles

Crystallite size and microstrain values for Yb_2O_3 were determined via line profile analysis of the XRPD data using integral breadth methods (Williamson–Hall, as well as Rietveld procedure) and by Fourier analysis (Warren–Averbach technique). The joined Rietveld refinement and size–strain analysis were performed using the Fullprof program [6] suite. The MarqX computer program [7] was used for the application of the Williamson–Hall and Warren–Awerbach methods. Instrumental broadening was fully characterized through the instrumental resolution function (IRF) that had been obtained using LaB_6 standard.

The results of all three methods used for microstructure analysis are given in Table 1. Bold numbers denote the originally obtained data for the corresponding method, while other values were calculated according to the following relations: $\langle D_V \rangle = 4\varepsilon_\beta/3$; $\langle D_A \rangle = 3\varepsilon_F/2$; $e_{r.m.s.} = (2/\pi)^{1/2} e$. $\langle D_V \rangle$ and $\langle D_A \rangle$ represent volume and area–weighted mean crystallite sizes. The relations between root-mean-square strain and maximum strain hold only under the assumption of a Gaussian-like strain distribution. From the crystallite size and strain values listed in Table 1 it can be deduced that crystallite size effects are the main source of peak broadening.

Using the Fullprof program, X-ray line broadening was analyzed by both the refinement of regular TCH-pV function parameters (isotropic effects), and the refinement of multipolar functions, i.e., symmetrized cubic harmonics (anisotropic effects) [8]. A better fit was obtained by allowing for anisotropic size effects. The deviations of the calculated average apparent size in different directions are small, indicating that crystallites are spherical in general. A projection of the surface representing the "average apparent size" on the crystallographic (0 0 1) plane is given in Fig. 3.

The different XRPD line profile size–strain analysis approaches produced very similar results for the crystallite size of Yb_2O_3. The microstrain values obtained via line profile analysis are within the same order of magnitude. The resulting mean microstrain (6×10^{-4}) suggests a low concentration of defects within the crystallites.

Table 1
Crystallite size and strain for nanosized Yb_2O_3.

Method	ε_β [nm]	ε_F [nm]	D_V [nm]	D_A [nm]	$\eta \times 10^4$	$e \times 10^4$	$e_{r.m.s.} \times 10^4$
MarqX: Line profile analysis with whole pattern fitting and pseudo-Voigt function							
Williamson–Hall plot	**13.8(2)**		18.4(3)		**8(5)**	2(1)	
Size–strain plot	**14(1)**		19(1)			8(7)	**6(6)**
Warren–Averbach analysis		**11.9(2)**		17.8(3)			
Fullprof: Line profile analysis with whole pattern fitting and TCH pseudo-Voigt function							
	13(2)					**5.7(1)**	

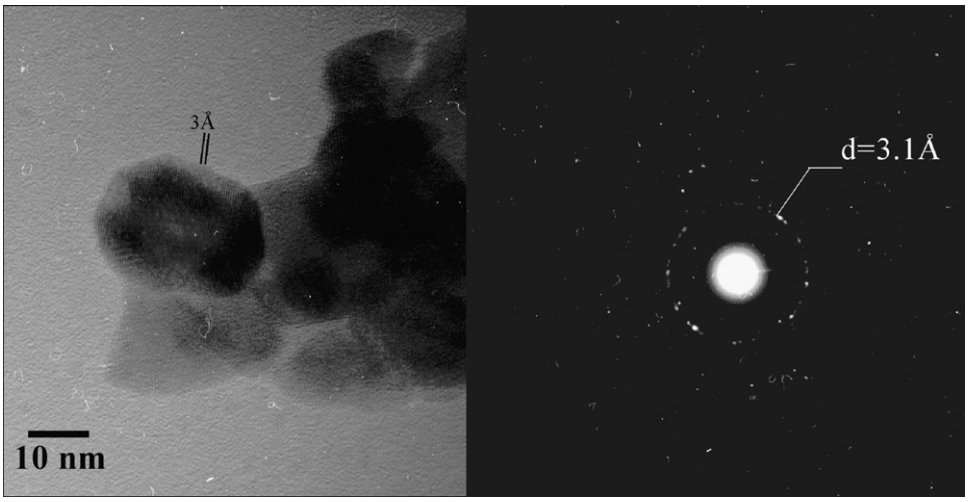

Fig. 3. HRTEM image of Yb_2O_3 particles (left) and the corresponding selected area electron diffraction (SAED) pattern (right).

3.3. Raman spectroscopy investigations of particles core and particles surface

The Raman spectrum of Yb_2O_3 nanoparticles collected using 632 nm excitation line is presented in Fig. 4. This spectrum is very similar to the spectra collected using two other excitation lines (488 and 514 nm – not shown). This spectra similarity was expected due to the sufficient penetration depth allowing observation of whole particle i.e., the core and the shell.

In analysis of Raman spectrum we focused on the region between 250 and 500 cm^{-1}, shown in the inset of Fig. 4. The main peak located at cc. 360 cm^{-1} is asymmetric and can be decomposed in nine components. We observed more than 15 peaks in the nano sample, while only five bands have been noticed in the study of the bulk Yb_2O_3 [9,10], (see, Table 2). Another study of Raman spectrum on cc. 60–65 nm-Yb_2O_3 by Dilawar et al. [11] also showed just slightly different spectrum (Table 2). However, numerous other studies showed the significant difference in the number of Raman bands of studied samples with literature data points to more pronounced structural differences. To clarify these differences, an interesting comparison was made with the Raman spectra of Gd_2O_3 in bulk form [12]. For this oxide two different modifications have been reported: a cubic phase (space group $Ia\bar{3}$) characterized by 6 peaks in the Raman spectrum (similar as in bulk Yb_2O_3), and a monoclinic form showing a total of 13 bands [12]. Most of the peaks of the latter phase compare well with the extra bands we observed for 25 nm-Yb_2O_3 specimen (Table 2, Fig. 4). A probable explanation is that the particles show core/shell structure with different structure type of core and shell. Core structure of the nanoparticles has cubic symmetry as shown by XRPD, while the shell regions show a monoclinic distortion or contain both cubic and monoclinic unit cells. Reported vibrations for nanostructured Yb_2O_3 (last column, Table 2) could be correlated with mixture of vibrations for monoclinic and cubic Gd_2O_3 (first and second columns), e.g. 362 cm^{-1} for core (C-type of structure) and 385 cm^{-1} for shell (monoclinic type of structure) of nanocomposed Yb_2O_3. It is probable that shell volume is rather small. Therefore, some vibrations e.g. those below 300 cm^{-1} are below the baseline or could not be deconvoluted.

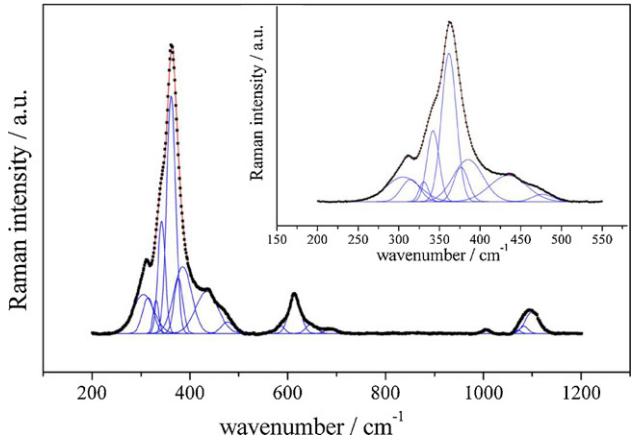

Fig. 4. Fit of the Raman spectrum of Yb_2O_3. Inset: details of the 250–500 cm^{-1} range.

An inspection of the fit (see inset of the Fig. 4) point to the existence of two type of vibration bands with different FWHM (the full widths at half maximum) of the bands, ranging from 13 to 53 cm^{-1}. This observation could be ascribed by the existence of a two phase mixture composed of an ordered (monoclinic or monoclinic/cubic) and a highly distorted material. Band broadening is intrinsic to many nanophased oxides because the small particle size hinders phonon propagation and hence induces a Brillouin zone folding which makes all phonons Raman active [13]. However, inspection of the literature data indicates that in the rare-earth sesquioxides Raman band broadening increases as the ionic radii

Table 2
Raman band wavenumbers ($\tilde{\nu}$) for Yb_2O_3.

Gd_2O_3 [12] monoclinic	Gd_2O_3 [12] cubic	Yb_2O_3 [11]	Y_2O_3 [13]	Y_2O_3:Yb [13] 950 °C	Y_2O_3:Tm [13] 950 °C	Yb_2O_3 [9]		Yb_2O_3 this work
						s1[a]	s2[b]	
219m								
233w	235w							
257w				256vw				
268w								
298m	299vw							
		307m						305m
	316m							314m
				326m	332vw			331m
	337vw	342m		339sh				342m
385s	361vs	365s	378vs	378vs	380vs	363vs	364vs	362vs
								377m
								385m
	401w							
415m		428w						
428m	435sh			433w	434w			435m
441m	447m	461w						
	479vw			470m	471w			477w
482m								
499w								
514vw				522w				
				545vw				
				560w				
588vw	568m			602w	602vw			586w
						611m	609m	614m
					631m			
				642w	649sh			648w
				681m				
				693sh		698w		685w
				720vw				
				762w		778vw		
				854w		860w		
								1006vw
								1071vw
								1083w
								1100m

vw – very weak; w – weak; m – medium; s – strong; vs – very strong; sh – shoulder.
[a] Coprecipitation synthesis.
[b] Combustion synthesis.

of the rare-earth atom is increasing [9]. An inspection of the ICSD crystal structure database [8] shows that with decreasing rare-earth ionic radius the octahedral distortion increases. Therefore, observed Raman band broadening in nanostructured Yb_2O_3 could be due to local structural distortions as well as the nanophase character of the sample. Both effects are significant and can be hardly separated, since Raman spectroscopy is less sensitive in determining the size effects in this case. The reason for not observing the core/shell structure of the nanoparticles with HRTEM and XRPD is most probably small distortion of the shell from the cubic symmetry, which was detected by very sensitive Raman spectroscopy, but is too small to be detected by HRTEM or XRPD.

Additionally, we checked presence of residuals of organic phase on the surface of the particles. By inspection of Raman spectra as well as IR spectra (not shown) in the whole range of record clearly indicates that any organic phase on the surface of the particles could be excluded. Moreover, similarity of here presented spectra on compounds obtained by decomposition of organometalic precursor with spectra on $(Yb,Y)_2O_3$ specimens obatined by mechanochemistry (free of orgnaic phase) [13], support this conclusion.

Well crystallized monoclinic Yb_2O_3 were produced under high pressure and under high temperature [14–16]. However, it is well know that in the particle surface chemical bonds are broken, translational symmetry is lost and coordination is changed. Observing monoclinic Raman bands indicated that nanoparticle surface is with monoclinic like structure. The other reason to observe monoclinic shell is that materials prepared from a liquid precursor have a structure very similar to that obtained by quenching from the high temperature melt. This effect has been demonstrated for many oxide compositions. The reason is that geometric/steric criteria are dominant in liquid phase and quenching from the liquid state or precipitation from liquid precursor keeps the orientational disorder of the liquid state. Thermal treatment is then necessary to develop the effect of coulombic long range interaction [17].

4. Conclusions

The synthesis route for controlled preparation of ytterbium sesquioxide with low concentration of defects is used. The applied method is straightforward, morphology and particle size are controlled starting from prepared acetylacetone (acac) complexes and by applying the same temperature-time heating regime. Synthesis of crystalline nanopowders directly from liquid organic precursor is important from the application point of view. The procedure reported here could be used for commercial production nanophosphors (such as $Yb:Y_2O_3$ and $Eu:Y_2O_3$) with low concentration of defects. Core and shell structure of 25 nm-Yb_2O_3 was determined by X-ray powder diffraction, HRTEM and Raman spectroscopy techniques. We demonstrated how by combining XRPD, HRTEM and Raman spectroscopy it was possible to extract information on existence of particle shell. Both X-ray and electron diffraction that are "sensitive" only to crystalline structures showed exclusive presence of cubic phase. However, Raman bands corresponding to both cubic and monoclinic symmetry were found. It should be taken into account that Raman spectroscopy is "sensitive" on both crystalline and amorphous structures. Therefore, the Raman spectrum

of 25 nm-Yb_2O_3 is composed of mixture of vibrations originating from both core and shell of nanoparticles.

Acknowledgment

This work has financially supported by both the Serbian Ministry of Science and Technology and SCOPES project (Grant No. IZ73Z0_1 27961). One of us (A.K.) would like to acknowledge the financial support from the CEEPUS project CII-AT-0038-01-0506-M-2329 as well as L'Association des Diplômes de l'Enseignement supérieur Français – ADEF.

References

[1] J.-P. Cuif, E. Rohart, P. Macadiere, C. Bauregard, E. Suda, B. Pacaud, N. Imanaka, T. Masui, S. Tamura, in: G. Adachi, N. Imanaka, Z.C. Kang (Eds.), Binary Rare Earth Oxides, Kluwer Academic Publishers, New York, 2004, pp. 215–256.
[2] J. Blanusa, B. Antic, A. Kremenovic, A.S. Nikolic, L. Mazzerolles, S. Mentus, V. Spasojevic, Solid State Commun. 144/7-8 (2007) 310.
[3] K. Takaichi, H. Yagi, J. Lu, J.F. Bisson, A. Shirakawa, K. Ueda, T. Yanagitani, A.A. Kaminskii, Appl. Phys. Lett. 84 (2004) 317.
[4] M. Marezio, Acta Crystallogr. 20 (1966) 723.
[5] Inorganic Crystal Structure Database, National Institute of Standard and Technology, Gaithersburg, version 1.4.4, 2008.
[6] J. Rodriguez-Carvajal (2008) FullProf computer program; FullProf computer program (http://www.ill.eu/sites/fullprof/index.html).
[7] Y.H. Dong, P. Scardi, J. Appl. Cryst. 33 (2000) 184.
[8] V. Honkimäki, P. Surotti, in: R.L. Snyder, J. Fiala, H.J. Bunge (Eds.), Defect and Microstructure Analysis by Diffraction, Oxford Univer. Press, New York, 1999, pp. 41–58.
[9] J.-C. Panitz, J. Raman Spectrosc. 30 (1999) 1035.
[10] J.-C. Panitz, J.-C. Mayor, B. Grob, W. Durisch, J. Alloys Compd. 303–304 (2000) 340.
[11] N. Dilawar, S. Mehrotra, D. Varandani, B.V. Kumaraswamy, S.K. Haldar, A.K. Bandyopadhyay, Mater. Charact. 59 (2008) 462.
[12] C. Le Luyer, A. Garcia-Murillo, E. Bernstein, J. Mugnier, J. Raman Spectrosc. 34 (2003) 234.
[13] A. Kremenovic, J. Blanusa, B. Antic, Ph. Colomban, V. Kahlenberg, C. Jovalekic, J. Dukic, Nanotechnology 18 (2007) 145616.
[14] G. Brauer, in: L. Eyring (Ed.), Progress in the Science and Technology of the Rare Earths, Vol.3, Pergamon, Oxford, 1968.
[15] H.R. Hoekstra, K.A. Gingerich, Science 146 (1964) 1163.
[16] B. Guo, A.S. Harvey, J. Neil, I.M. Kennedy, A. Navrotsky, S.H. Risbud, J. Amer. Ceram. Soc. 90 (2007) 3683.
[17] Ph. Colomban, Nano/microstructure and Properties control of single and multiphase materials, in: B. Lee, S. Komarneni (Eds.), Chemical Processing of Ceramics, 2nd ed., CRC, Taylor & Francis, 2005 (Ch12).